Evolution of hexagonal lateral ordering in strain-symmetrized $PbSe/Pb_{1-x}Eu_xTe$ quantum-dot superlattices

M. Pinczolits, G. Springholz,* and G. Bauer
Institut für Halbleiterphysik, Johannes Kepler Universität, A-4040 Linz, Austria
(Received 29 April 1999; revised manuscript received 8 July 1999)

Lateral ordering and size homogenization of self-organized PbSe quantum dots in strain-symmetrized $PbSe/Pb_xEu_{1-x}Te$ superlattices is studied using atomic force microscopy. For superlattices with the number of superlattice periods varying from $N=1$ to 100 it is found that a nearly perfect hexagonal two-dimensional (2D) lattice of PbSe dots is formed on the surface already after a few periods. A detailed analysis of the dot arrangement shows that within these superlattices, the in-plane spacing of the dots as well as the dot sizes within each PbSe layer remain essentially constant throughout the whole superlattice growth. This marked different behavior as compared to other self-assembled quantum dot superlattice systems is explained by the special ordering mechanism in our material system that is characterized by the formation of a non-vertical alignment of the PbSe dots in the superlattice stack due to the very high elastic anisotropy of the IV-VI semiconductors. In addition, from *in situ* reflection high-energy electron diffraction measurements it is found that the critical coverage for PbSe islanding, and thus the material distribution between the wetting layer and the islands are not changed within the stack. Therefore, remarkable homogenous three-dimensionally ordered quantum dot arrays are formed. [S0163-1829(99)02139-6]

I. INTRODUCTION

The spontaneous formation of three-dimensional (3D) islands in strained layer heteroepitaxy has recently evolved as a technique for the fabrication of self-assembled quantum dots.[1–3] It is based on the fact that for highly strained heteroepitaxial layers an abrupt transition from two-dimensional to 3D growth occurs in the Stranski-Krastanow growth mode, with the formation of coherent islands on the surface after completion of the 2D wetting layer. Such defect-free islands embedded in a higher band-gap matrix material have proven to exhibit excellent electronic properties due to the effective quantum confinement of the charged carriers in all three directions. For practical device applications, however, the considerable variations of size and shapes within the large ensemble of quantum dots has remained a critical issue.

In multilayers of self-assembled quantum dots, theoretical,[4,5] as well as experimental work[6–9] has shown that the vertical interaction of dots via their elastic strain fields[10,11] may lead to a gradual improvement in size homogenity, as well as to a more uniform lateral island spacing. This self-organization is a result of the overlap of the localized strain fields of neighboring buried islands, with a preferred nucleation of subsequent islands on the surface where the elastic energy exhibits a local minimum.[4,10,12] However, in SiGe/Si or InAs/GaAs quantum dot superlattices, it has been found that in spite of the lateral ordering tendency between vertical columns of self-assembled dots, a substantial increase of the island size as well as lateral island separation occurs during superlattice growth.[6,7] Even more, several groups have observed a shift of the onset of 3D island formation to smaller critical coverages of the wetting layer as the superlattice growth proceeds.[13,14] This was attributed to surface segregation as well as to the influence of the local strain fields of buried islands. As a consequence, the partition of the dot material between the wetting layer and the quantum dot islands changes with increasing number of superlattice periods. Thus, in spite of the lateral ordering tendency in each dot layer, the overall size homogenity in the multilayers is not necessarily improved. In addition, the degree of lateral ordering achieved up to now has been rather limited. Furthermore, because of the existing lattice misfit between the superlattice stack and the substrate or buffer layer, strain relaxation and defect formation sets in after the growth of a few superlattice periods, as shown, e.g., in Ref. 15. This results in changes of the electronic properties if a critical number of periods is exceeded, and poses severe limitations on the number of superlattice periods that can be deposited in order to induce a lateral ordering of the 3D islands during growth.

In the present paper, we have studied the evolution of lateral ordering in self-assembled quantum dot $PbSe/Pb_xEu_{1-x}Te$ superlattices. In these structures, the layer thicknesses and the composition of the $Pb_xEu_{1-x}Te$ spacer layers were adjusted to achieve a full strain-symmetrization of the superlattice stack with respect to the PbTe buffer layer. This allows the fabrication of superlattices with an arbitrary number of periods without changes in the strain status of the layers and without risk of misfit dislocation formation. We find that a particularly efficient lateral ordering of the PbSe dots takes place, with the formation of a nearly perfect hexagonal 2D lattice of dots already after a few superlattice periods. A detailed analysis of the evolution of the dot arrangement by atomic force microscopy (AFM) reveals that the dot sizes, the dot spacing and the wetting layer thickness are essentially constant throughout the whole superlattice stack. Therefore, remarkable homogenous 3D quantum dot arrays are formed. This is explained by the nonvertical alignment and the *ABCABC* vertical stacking sequence of the PbSe dots in the superlattices that arise from

the very high elastic anisotropy of the IV-VI semiconductor materials.[12]

II. EXPERIMENT

The samples were grown by molecular-beam epitaxy on 2–4 μm fully relaxed PbTe buffer layers predeposited on (111) oriented BaF_2 substrates. For all samples, the superlattice stack consisted of 5 monolayers (ML) PbSe alternating with 470 Å of $Pb_xEu_{1-x}Te$, using growth rates of 0.08 ML/s and 3.5 Å/s, respectively, and a substrate temperature of 360 °C. The evolution of surface structure and surface morphology was monitored by *in situ* reflection high-energy electron diffraction (RHEED) during growth using an electron gun operated at 35 keV. To study the evolution of lateral ordering, samples with superlattice periods from $N=1$ to 100 were prepared, where the last PbSe quantum dot layer was left uncapped for further analysis. After growth, the samples were rapidly cooled to room temperature to freeze in the epitaxial surface morphology. The surface structure was imaged by atomic force microscopy (AFM) directly after removal of the samples from the molecular-beam epitaxy system. AFM measurements were carried out using an AutoProbe CP AFM and sharpened Micro- and Ultralevers of Park Scientific Instruments. Special image processing software was developed for real-space statistic analysis of the dot size distributions on the one hand, and for frequency space analysis of the degree of lateral ordering using fast Fourier transformation and autocorrelation function analysis.

III. SAMPLE STRUCTURE

A crucial aspect of our work was the adjustment of the ternary composition of the $Pb_{1-x}Eu_xTe$ spacer layers, in order to achieve a full strain symmetrization between the *tensily* strained PbSe layers and the *compressively* strained $Pb_{1-x}Eu_xTe$ layers. If the in-plane lattice-constant $a_{\parallel,\mathrm{free}}$ of the free-standing superlattice stack matches the lattice constant a_s of the PbTe buffer layer, an arbitrary number of superlattice periods can be deposited on the buffer layer without misfit dislocation formation and without a change in the strain status of the epitaxial layers as growth proceeds. Since the PbSe dot layers are under tensile strain (lattice mismatch of -5.54% with respect to the PbTe buffer layer), strain symmetrization can be achieved only by using a spacer layer material that has a lattice constant larger than PbTe. This is the case for the ternary $Pb_{1-x}Eu_xTe$, for which the lattice constant increases (nonlinearly) with increasing Eu content.[16]

For pseudomorphic 2D superlattices with coherent interfaces, the in-plane lattice constant $a_{\parallel,\mathrm{free}}$ that is assumed by a free-standing superlattice stack removed from its substrate is determined by the minimization of the total strain energy. For a given in-plane lattice constant $a_{\parallel,\mathrm{SL}}$ within the superlattice, the in-plane strain in each layer is given by:

$$\epsilon_i=\frac{(a_{\parallel,\mathrm{SL}}-a_{0,i})}{a_{0,i}}, \tag{1}$$

where $a_{0,i}$ is the bulk lattice constant of the layer material i. The total strain energy E_{strain} in a superlattice stack with N periods is then given by

$$E_{\mathrm{strain}}=N(M_1\epsilon_1^2+M_2\epsilon_2^2), \tag{2}$$

where M_i are the elastic energy moduli of the biaxially strained layers, which are determined by the elastic constants of the layer materials and by the growth orientation (axis of the biaxial strain). For the (100) growth orientation, $M=(c_{11}-c_{12})(c_{11}+2c_{12})/c_{11}$, and for (111) growth $M=6c_{44}(c_{11}+2c_{12})/(c_{11}+2c_{12}+4c_{44})$ (Ref. 17) with c_{ij} being the elastic constants of a cubic material. The in-plane lattice constant $a_{\parallel,\mathrm{free}}$ of a free-standing superlattice is then obtained from the minimization of the total strain energy with respect to $a_{\parallel,\mathrm{SL}}$, which leads to the condition that the strain-thickness product $\epsilon_{\parallel,i}d_i$ of the two individual superlattice layers is roughly equal, or more precisely,

$$(\epsilon_{\parallel,1}d_1)/(\epsilon_{\parallel,2}d_2)=K. \tag{3}$$

$\epsilon_{\parallel,i}$ are the in-plane layer strains of the two layers, which are related to $a_{\parallel,\mathrm{free}}$ by $\epsilon_{\parallel,i}=(a_{\parallel,\mathrm{free}}-a_i)/a_i$ and K is a constant that is determined only by the elastic energy moduli and the elastic constants of the layer materials with $K=(M_1/a_1)/(M_2/a_2)$. For the $PbSe/Pb_xEu_{1-x}Te$ superlattices considered here, $K=1.32$ ($i=1$ for PbSe and $i=2$ for $Pb_{1-x}Eu_xTe$), and it is close to one also for many other materials combinations.

For a strain-symmetrized superlattice, $a_{\parallel,\mathrm{free}}$ must be equal to the lattice constant of the substrate or buffer layer a_s. Then, $\epsilon_{\parallel,i}$ are just given by the lattice mismatch of the layer materials with respect to a_s, and Eq. (3) defines the thickness ratio between the layers required to fulfill the strain symmetrization condition. For our dot superlattices, where the material and thickness of the dot layer (5 ML PbSe) as well as the $Pb_{1-x}Eu_xTe$ spacer thickness (470 Å) was fixed, strain-symmetrization is achieved for $\epsilon_{\parallel,\mathrm{PbEuTe}}=0.245\%$, i.e., a $Pb_{1-x}Eu_xTe$ ternary composition of $x=0.07$. Although, Eq. (3) is strictly valid only for 2D multilayers, high-resolution x-ray diffraction spectra show that for the such determined parameters the main superlattice diffraction peak of our dot samples coincides with that of the PbTe buffer layer. Thus, this expression is a good approximation for the strain-symmetrization condition in quantum dot superlattices as well.

IV. RESULTS

The evolution of surface structure during superlattice growth was monitored by *in situ* reflection high-energy electron diffraction (RHEED). Figure 1 shows the the specular spot intensity and of two 3D transmission diffraction spots recorded during the growth of the first and 30th PbSe layer in a $PbSe/Pb_xEu_{1-x}Te$ superlattice (full and dashed lines, respectively) as a function of PbSe coverage. Also shown are the RHEED patterns before and after the onset of 3D islanding at 0.5 and 4 ML PbSe coverage (top panel of Fig. 1). During the growth of the PbSe wetting layer, the RHEED intensities remain constant and equal to that of the 2D $Pb_{1-x}Eu_xTe$ spacer layer. At a critical coverage of 1.4 ML, weak chevron-shaped 3D transmission spots start to appear in the RHEED patterns, but an abrupt transition to a 3D transmission diffraction pattern takes place only at 2.3-ML coverage where the specular spot completely disappears.

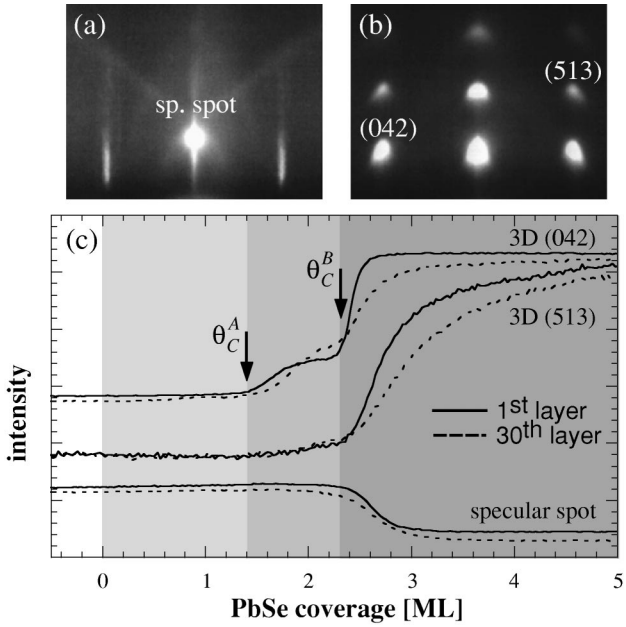

FIG. 1. Top panel: RHEED patterns observed during the PbSe dot layer growth of a PbSe/Pb_xEu_{1-x}Te superlattice structure of PbSe coverages of 0.5 (a) and 4 monolayers (b). Lower panel (c): Evolution of the intensity of the specular spot and the (513) and (042) transmission spots during the growth of the first and the last PbSe layer of a 30-period PbSe/Pb_xEu_{1-x}Te superlattice plotted as a function of PbSe coverage. The arrows indicate the critical coverages for 3D islanding at $\theta_c^A = 1.4$ and $\theta_c^B = 2.3$ monolayers.

During the growth of the $Pb_{1-x}Eu_xTe$ spacer layers, the intensity changes are reversed and a 2D reflection diffraction image is recovered after about 200-Å-layer thickness. Thus, a 2D surface is restored once the PbSe islands are completely buried by the spacer layer.

As is evident from Fig. 1, the characteristic two-step islanding process during PbSe growth[18] and the 2D surface recovery during the spacer growth are exactly reproduced during each superlattice period, and even after 30 periods, the same *absolute* intensity changes take place. In particular, the critical coverage at which PbSe islanding occurs remains constant throughout superlattice growth, indicating that the distribution of material between the wetting layer and the islands does not change within the superlattice stack. In addition, the RHEED measurements also indicate that the coverage at which the PbSe islands are completely buried by the 2D spacer layer remains constant. This is a first indication that the PbSe island size does not change significantly during superlattice growth.

Figure 2 shows a series of AFM images of the last uncapped PbSe dot layer of samples consisting of $N = 1$, 10, 30 and 100 superlattice periods. For the single layer [Fig. 2(a)], the PbSe islands are distributed randomly on the surface without any preferred lateral correlation direction. With increasing number of superlattice periods, a rapidly progressing ordering of the dots occurs. Already after 10 periods, the dots are preferentially aligned in single and double rows along the $\langle \bar{1}10 \rangle$ directions on the surface [Fig. 2(b)]. Measurements on samples with less than 10 bilayers show that

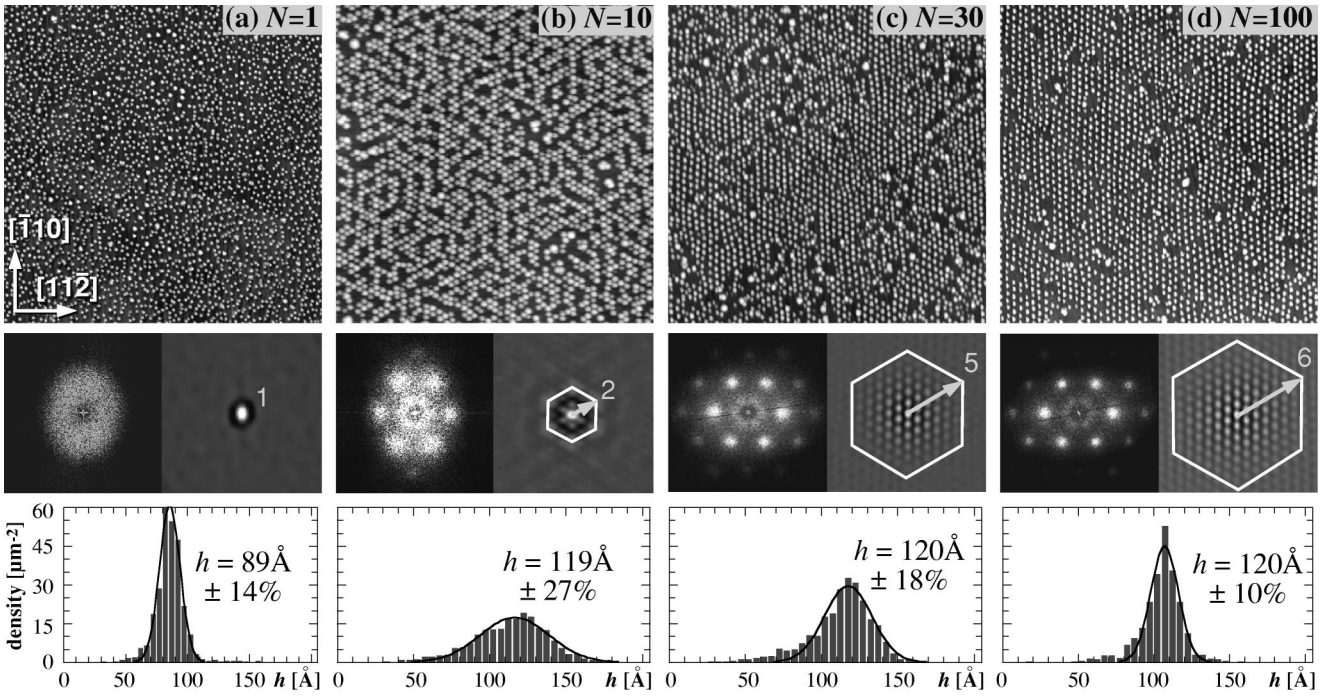

FIG. 2. Upper panel: Atomic force microscopy images ($3 \times 3\ \mu m^2$) of (a) a single layer of self-assembled PbSe quantum dots and of the last PbSe layer of PbSe/Pb_xEu_{1-x}Te superlattice stacks with a number of superlattice periods of 10 (b), 30 (c), and 100 (d). Center panel: Corresponding Fourier transform power spectra (left side) and autocorrelation spectra ($1 \times 1\ \mu m^2$, right side). Lower panel: Height histograms of the PbSe dots determined from the AFM images. The abscissae indicate the dot height, the ordinates the areal dot density, and the full lines are Gaussian fits of the histograms.

this ordering commences first with the formation of small patches of hexagonally ordered regions, which subsequently enlarge and join to form row-type structures. With further increasing number of bilayers, larger and larger ordered regions are formed [see Figs. 2(c) and 2(d)]. For samples with $N>30$, the perfect hexagonal arrangement is disrupted only by single-point defects, such as missing dots, dots at interstitial positions, or occasionally, by additionally inserted dot rows (''dislocations'').

The development of the lateral ordering was determined by Fourier transformation (FFT) as well as auto correlation (AC) analysis of the AFM images as shown in the center panel of Fig. 2. Whereas the FFT power spectra yield information on preferred spatial frequencies, the AC spectra indicate the degree of self-similarity in the real-space images, i.e., in our case the lateral extent of the ordered dot domains. The FFT power spectrum of the $N=1$ single dot layer AFM image exhibits a broad ring around the frequency origin. By fitting cuts through the ring in several directions with Gaussians, we obtain a mean peak position of about 12.5 μm^{-1} corresponding to an average dot distance of 800 Å. The relative width (FWHM) of this ring of $\pm 47\%$ indicates a substantial variation of the lateral dot separation. This width is essentially independent of the surface direction, i.e., no preferred lateral alignment of the islands exists in any surface direction. In addition, the AC spectrum of the AFM image (see Fig. 2) does not exhibit any structure outside of the central maximum, indicating the lack of any lateral correlation of the dot positions.

In contrast, the FFT power spectrum of the 10 bilayer sample [Fig. 2(b)] clearly shows six pronounced side maxima, corresponding to a mean spacing of the dot *rows* of 590 Å along $\langle 11\bar{2}\rangle$. Side maxima appear also in the AC spectrum, which indicates that the next-nearest neighbors of the dots are aligned along the $\langle \bar{1}10\rangle$ directions, with a preferred dot-dot distance of 680 Å within the rows. Apart from the six side maxima, the FFT power spectrum also exhibits a well defined ring at a special frequency of one-third of the side peaks, and this ring also exhibits a hexagonal symmetry. From a closer inspection, it is found to be due to the ''missing rows'' in the dot arrangement, which forms a (3×1)-like missing-row ''superstructure'' because on average every third dot row is missing [see Fig. 2(b)].

For the 30- and 100-period superlattices, the peaks in the FFT spectra drastically sharpen, and many higher-order satellite peaks are observed [Figs. 2(c) and 2(d), respectively]. As shown in Fig. 3(b), the relative FWHM of the satellite peaks, mainly reflecting the variation of the mean dot-dot distance, narrows from about $\pm 47\%$ for the single layer to $\pm 6\%$ for the 100-period superlattice, i.e., the dot-dot spacing during superlattice growth becomes increasingly well defined. In addition, the AC spectra reveal the formation of large perfectly ordered dot domains, with a correlation of the dot position over up to ten nearest-neighboring dots. In order to determine the average domain size of the ordered regions, the heights of the side peaks along the $\langle \bar{1}10\rangle$ directions in the AC images were determined. Defining a domain cutoff where the peak height is reduced to one tenth of the central maximum, average domain radii of 1, 2, 5, and 6 times the average dot spacing are obtained for the superlattices with

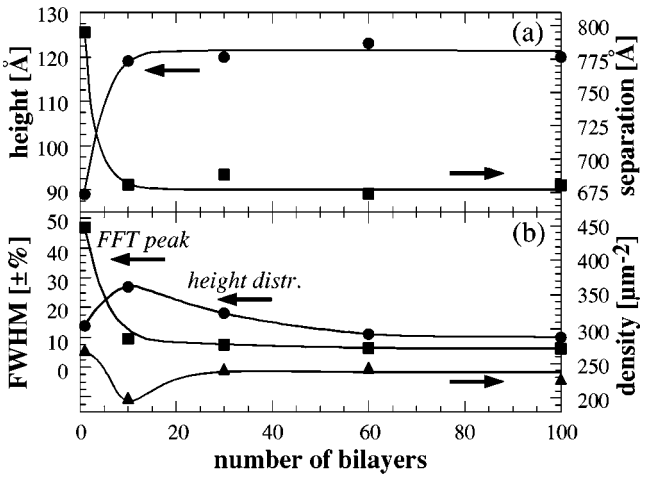

FIG. 3. Dot parameters plotted as a function of the number of $PbSe/Pb_xEu_{1-x}Te$ superlattice periods: (a) Average height (dots, left ordinate) and average lateral separation of dots in the $\langle \bar{1}10\rangle$ directions determinded from the separation of the satellite Fourier peaks (squares, right ordinate). (b) Full width at half maximum (FWHM) of the satellite FFT peaks and of the dot-height distributions (dots and squares, respectively, left ordinate), and areal density of the PbSe dots (triangles, right ordinate).

$N=1$, 10, 30, and 100 periods, respectively. The corresponding domain sizes are indicated by the hexagons in the AC images of Fig. 2.

So far, we have addressed only the lateral ordering tendency of the PbSe dots. To gain information on the influence of ordering on the dot size variation, we analyzed the evolution of the island height distribution as a function of the superlattice periods. The lowest panel in Fig. 2 shows the Gaussian-fitted height histograms of the PbSe dots determined from the statistical evaluation of several 2×2-μm^2 AFM images with a minimum of 750 single PbSe dots for each sample. The obtained average island heights and the height variations are plotted in Figs. 3(a) and 3(b), respectively, versus number of superlattice periods. For the single PbSe dot layer, at 5 ML coverage the average island height is 89 Å with a variation of $\pm 14\%$. In spite of the fact that lateral ordering sets in already after the first few superlattice periods, the dot height distribution at first actually broadens to $\pm 27\%$ after 10 superlattice periods, and only thereafter decreases to reach a value of of $\pm 10\%$ for $N=100$. A complementary transient behavior is observed for the areal dot density [see Fig. 3(b)], which at first decreases up to 10 bilayers and then gradually increases again for higher N. With respect to the island shapes, we find no indication that the ordering process influences the dot shape, i.e., the threefold {100} faceted pyramidal shape already determined for the single layers[18] remains unchanged.

V. DISCUSSION

In contrast to the vertical alignment observed for III-V and group-IV quantum dot multilayers,[8–11] the layer-to-layer dot correlation in our $PbSe/Pb_xEu_{1-x}Te$ quantum dot superlattices is not parallel but *inclined* to the growth direction.[12] As shown by theoretical calculations, this is due to the very high elastic anisotropy of the IV-VI lead salt materials as

well as the chosen (111) growth orientation.[19] As a result, fcc-like *ABCABC* vertical stacking sequence is formed in the superlattices where the lateral dot separation within the PbSe dot layers is *exactly* defined by the thickness of the $Pb_{1-x}Eu_xTe$ spacer layer.[12] This is due to the fact that the inclined interlayer dot correlation angle of 39° with respect to the surface normal is independent of the spacer layer thickness, as was determined by high-resolution x-ray diffraction.[12] For the constant $Pb_{1-x}Eu_xTe$ spacer thickness of 470 Å in the superlattice samples of this work, this correlation angle leads to a preferred lateral separation of the dots of 680 Å within the growth plane, which corresponds to a dot density of 250 μm^{-2} for a perfect hexagonal 2D dot lattice. As shown in Fig. 3, this is indeed the dot separation and density observed for the superlattice samples with more than 30 superlattice periods.

The initial transient behavior of the dot density as well as the initial increase of the dot-size variation in the superlattices can therefore be understood in terms of a *mismatch* of the areal dot density in the first PbSe layer with respect to the preferred density in the dot superlattices. The former is determined only by the growth conditions and the PbSe layer thickness.[18] As is evident from the AFM image of the 10-period superlattice, this lattice misfit is initially accommodated by a high density of defects and missing rows in between hexagonally ordered dot regions. These defects and missing rows are not only the origin for the decrease in the overall dot density, but also cause an initial increase of the dot-size variation, because the size of the dots near defects is found to deviate from those within the ordered regions. On the other hand, once the preferred lateral dot separation is enforced after a sufficient number of superlattice periods, with decreasing defect density in the 2D dot lattice a substantial improvement of the overall size homogenity within the dot layers occurs.

This interpretation is further supported by the dependence of the lateral dot separation on the number of superlattice periods shown in Fig. 3(a), as determined from the separation of the satellite peaks in the FFT images. Clearly, one can see that even for the 10-period superlattice, the lateral dot separation *within* the ordered regions is already equal to the fixed value of 680 Å enforced by the spacer thickness, and the same value is also observed for the superlattices with larger number of periods. Therefore, a very rapid transition from the initial dot spacing, determined merely by the growth conditions, to the preferred dot spacing in the superlattice stack takes place. As is evident from Fig. 3(a), after this transition also the average PbSe dot height within each superlattice layer remains constant throughout the whole superlattice growth, which is another indication that the thickness of the wetting layer remains unchanged.

It is noted, that our results are in clear contrast to the observations for dot superlattices of other materials systems. For SiGe/Si dot superlattices, e.g., Teichert *et al.*[6] reported a *threefold* increase of the SiGe dot size and of the lateral dot spacing when the number of periods increases from $N=1$ to 30. In addition, an increase of dot size and dot spacing by a factor of 1.5 was reported for InAs/GaAs superlattices.[7] Even more, for these materials systems the size homogenization and the degree of lateral ordering in the dot superlattices was not very large. This marked different behavior is due to the different *vertical* correlation of the dots in these superlattices, in which due to the much smaller elastic anisotropy of the materials as compared to the IV-VI compounds the dots in the superlattice strongly tend to be aligned parallel to the growth direction. Our results provide clear evidence for the fact that the self-organization mechanism due to nonvertical dot correlations in superlattices is much more efficient than in systems where the dots are vertically aligned. This is in agreement with our recent theoretical studies described in Ref. 19.

VI. CONCLUSION

In conclusion, we have determined the evolution of lateral ordering in self-organized $PbSe/Pb_xEu_{1-x}Te$ quantum dot superlattices. Due to strain symmetrization, dot superlattices with large number of superlattice periods could be prepared without strain relaxation by misfit dislocation formation. From *in situ* reflection high-energy electron diffraction studies as well as atomic force investigations it was demonstrated that remarkable homogenous 3D ordered arrays of PbSe dots are obtained. In comparison to other dot superlattice materials systems, in our samples the in-plane spacing of the dots, the dot sizes, and the material distribution between the wetting layer and the islands remain essentially constant throughout the whole superlattice growth. This yields a significant improvement of the size homogenity of the quantum dots, which is of crucial importance for device applications.

ACKNOWLEDGMENTS

This work was supported by the ÖNB Jubiläumsfonds, the Fonds zur Förderung der wissenschaftlichen Forschung, and the Gesellschaft für Mikroelektronik, Austria.

*Electronic address: G.Springholz@hlphys.uni-linz.ac.at

[1] D. Leonard, M. Krishnamurty, C. M. Reaves, S. P. Denbaar, and P. Petroff, Appl. Phys. Lett. **63**, 3203 (1993).

[2] J. M. Moison, F. Houzay, F. Barthe, L. Leprince, E. Andre, and O. Vatel, Appl. Phys. Lett. **64**, 196 (1994).

[3] R. Noetzel, J. Temmyo, and T. Tamamura, Nature **369**, 131 (1994).

[4] J. Tersoff, C. Teichert, and M. G. Lagally, Phys. Rev. Lett. **76**, 1675 (1996).

[5] F. Liu, S. E. Davenport, H. M. Evans, and M. G. Lagally, Phys. Rev. Lett. **82**, 2528 (1999).

[6] C. Teichert, L. J. Peticolas, J. C. Bean, J. Tersoff, and M. G. Lagally, Phys. Rev. B **53**, 16 334 (1996).

[7] G. S. Solomon, S. Komarov, J. S. Harris, and Y. Yamamoto, J. Cryst. Growth **175/176**, 707 (1997).

[8] A. A. Darhuber, V. Holý, J. Stangl, G. Bauer, A. Krost, F. Heinrichsdorff, M. Grundmann, D. Bimberg, V. M. Ustinov, P. S. Kopev, A. O. Kosogov, and P. Werner, Appl. Phys. Lett. **70**, 955 (1997).

[9] V. Holý, A. A. Darhuber, J. Stangl, S. Zerlauth, F. Schäffler, G. Bauer, N. Darowski, D. Lübbert, U. Pietsch, and I. Vávra, Phys. Rev. B **58**, 7934 (1998).

[10] Q. Xie, A. Madhukar, P. Chen, and N. Kobayashi, Phys. Rev. Lett. **75**, 2542 (1995).

[11] G. S. Solomon, J. A. Trezza, A. F. Marshall, and J. S. Harris, Phys. Rev. Lett. **76**, 952 (1996).
[12] G. Springholz, V. Holý, M. Pinczolits, and G. Bauer, Science **282**, 734 (1998).
[13] Y. Nakata, Y. Sugiyama, T. Fuatsugi, and N. Yokoyama, J. Cryst. Growth **175/176**, 713 (1997).
[14] O. G. Schmidt, O. Kienzle, Y. Hao, K. Eberl, and F. Ernst, Appl. Phys. Lett. **74**, 1272 (1999).
[15] Q. Xie, N. P. Kobayshi, T. R. Ramachandran, A. Kalburge, P. Chen, and A. Madhukar, J. Vac. Sci. Technol. B **14**, 2203 (1996).
[16] D. L. Partin and C. M. Thrush, Appl. Phys. Lett. **45**, 193 (1984); A. Ishida, S. Matsuura, M. Mizuno, Y. Sase, and H. Fujiyasu, J. Appl. Phys. **63**, 4572 (1988).
[17] See, e.g., D. J. Bottomley and P. Fonds, J. Cryst. Growth **160**, 406 (1996).
[18] M. Pinczolits, G. Springholz, and G. Bauer, Appl. Phys. Lett. **73**, 250 (1998).
[19] V. Holý, G. Springholz, M. Pinczolits, and G. Bauer, Phys. Rev. Lett. **83**, 356 (1999).